

# Joint Source-and-Channel Coding for Small Satellite Applications

Olga Kondrateva  
Humboldt-Universität zu Berlin  
Berlin, Germany  
kondrate@informatik.hu-berlin.de

Stefan Dietzel  
Merantix Momentum GmbH  
Berlin, Germany  
stefan.dietzel@merantix.com

Björn Scheuermann  
Technical University of Darmstadt  
Darmstadt, Germany  
scheuermann@kom.tu-darmstadt.de

**Abstract**—Small satellites are widely used today as cost effective means to perform Earth observation and other tasks that generate large amounts of high-dimensional data, such as multi-spectral imagery. These satellites typically operate in low earth orbit, which poses significant challenges for data transmission due to short contact times with ground stations, low bandwidth, and high packet loss probabilities. In this paper, we introduce JSCC-SAT, which applies joint source-and-channel coding using neural networks to provide efficient and robust transmission of compressed image data for satellite applications. We evaluate our mechanism against traditional transmission schemes with separate source and channel coding and demonstrate that it outperforms the existing approaches when applied to Earth observation data of the Sentinel-2 mission.

**Index Terms**—cross-layer optimization; AI-enabled networking; small satellite applications

## I. INTRODUCTION

Over the last decade, small satellites have become an increasingly important part of the space industry. The main advantages of small satellites are their low cost and flexibility. In particular, the CubeSat standard [1] has become popular due to availability of commercial off-the-shelf (COTS) components, which considerably simplify and speed up the manufacturing. Originally, the use of CubeSats was limited to demonstration flights and education purposes. With technological advances, however, their application has expanded to a variety of important areas like Earth observation [2], communication systems [3], disaster management [4], and even to deep space missions. For example, small satellites are used as interplanetary relay for data, and they are used for monitoring the Earth's moon and planet Mars [5].

Since many space applications are inherently data-centric, large amounts of data need to be transmitted to Earth where they are then analyzed. Over the years, the resolution of satellite imagery has increased considerably. Many sensors produce multi-spectral images for a wide spectrum of wavelengths, by far exceeding visible light, which results in high-dimensional image data and consequently high communication demands. However, this demand for communication can barely be met with existing CubeSat technologies. CubeSats are typically put into low Earth orbit (LEO) and orbit the Earth several times a day. As a result, each satellite is in communication range of a ground station only four to five times per day

for short periods of around ten minutes each. Furthermore, CubeSats are extremely power-constrained devices, since their small size limits the area available for solar panels. Finally, due to severe weather conditions and the relatively high velocity of satellites, communication with ground stations is subject to high packet loss [6]. To properly utilize the available contact periods, and to compensate for satellite movement and changing weather conditions, a flexible and reconfigurable communication system is required.

Two major aspects of the communication system are source coding and channel coding. Source coding is used to reduce the overall amount of data that needs to be transmitted, and channel coding protects the data against errors that result from the harsh communication environment. Traditionally, source and channel coding are considered separately; for example, JPEG 2000 is used as a lossy compression scheme for source coding [7], and low-density parity-check (LDPC) can be used for channel coding.

Although Shannon's separation theorem [8] states that optimal results can be achieved when source and channel coding are treated separately, the theorem assumes an infinite code block length, whereas, in practice, we are limited to finite lengths. It is known that joint optimization of source and channel coding has the potential to achieve better practical communication performance [9]. While a number of joint coding approaches using optimization techniques exist [10]–[12], they are too complex to be practically applied [13]. Recently, neural networks have been proposed to learn a joint source and channel coding (JSCC) scheme for transmitting RGB images in a terrestrial communication setting [14].

In this paper, we introduce joint source-and-channel coding for small satellite applications (JSCC-SAT), which applies the idea of joint source and channel coding (JSCC) using neural networks to multi-spectral image data and adapts it to the challenging requirements of satellite communication. Using a neural network with an encoder-decoder architecture, the input data can be directly mapped to channel symbols, combining source coding, channel coding, and modulation. This approach has a number of important benefits, which are particularly useful for satellite communication. In contrast to general compression methods, a neural network can be trained on the specific data that is relevant for a use case, thereby taking the data's properties into account. Benefits of using neural

networks for source coding have already been demonstrated in literature [15]. As an additional benefit, JSCC mitigates the so-called “cliff effect,” a sudden loss of digital signal reception when signal strength decreases. Moreover, JSCC offers better performance in case of varying signal-to-noise ratios (SNRs) [14], and it adapts to different channel conditions [16]. Finally, it can provide incremental image quality updates [17], similar to JPEG 2000’s layering technique, which encodes multiple image qualities within a single file. Such incremental updates are particularly useful in the cases of partial transmissions due to short communication periods.

Our main contribution can be summarized as follows:

- We adapt joint source and channel coding (JSCC) using convolutional neural network (CNN) for compression and transmission of image data in small satellite applications (JSCC-SAT).
- We train a suitable example network using realistic Sentinel-2 Earth observation data and realistic signal-to-noise parameters for satellite communication.
- We show that JSCC-SAT provides better quality than source coding using JPEG 2000 combined with channel coding using LDPC for most parameter combinations.

The remainder of this paper is organized as follows. In Section II, we discuss related work on satellite image compression and joint coding approaches in other domains. We explain our application and communication setting in Section III followed by a detailed description of JSCC-SAT in Section IV. To evaluate JSCC-SAT, we compare it against separate source and channel coding in Section V, and we conclude the paper and give an outlook on future work in Section VI.

## II. RELATED WORK

In the following, we review existing mechanisms that perform JSCC with and without neural networks, in different application domains, as well as existing approaches that demonstrate the potential of neural networks for source coding alone.

JSCC received a lot of attention over the last years. Various cross-layer optimization approaches have been proposed to jointly optimize the parameters of source coding, channel coding, and modulation [10]–[12]. A similar approach was also proposed specifically for deep-space applications [18]. Their computation complexity, however, limits the applicability of these methods in practical scenarios.

To overcome this problem, deep JSCC based on encoder-decoder architecture has originally been proposed by Bourtsoulatzé et al. [14]. A benefit of JSCC using neural networks is that it mitigates the so-called “cliff effect,” a phenomenon that describes sudden significant decreases in image quality as the channel conditions change. In subsequent works, the basic approach has been improved to allow for using non-differentiable channel models [19], progressive transmission of images [17], transmission using a finite channel symbol alphabet (previous works assumed arbitrary complex values) [20], orthogonal frequency division multiplexing [21], adaptive rate control [16], transmission of correlated sources [22], and

TABLE I  
OVERVIEW OF SENTINEL-2 BANDS

Band	Measurement	resolution [m]
Band 1	Coastal aerosol	60
Band 2	Blue	10
Band 3	Green	10
Band 4	Red	10
Band 5	Vegetation red edge	20
Band 6	Vegetation red edge	20
Band 7	Vegetation red edge	20
Band 8	Near infrared	10
Band 8A	Narrow near infrared	20
Band 9	Water vapour	60
Band 10	Short wave infrared: cirrus	60
Band 11	Short wave infrared	20
Band 12	Short wave infrared	20

many others. All these works use general image databases for evaluation and do not take into account the specifics of satellite images. Furthermore, the authors consider terrestrial communication channels rather than the specifics of satellite communications, such as the dependency of SNRs on elevation angles.

Deep-learning-based methods were also proposed for source compression alone and are known to better preserve image quality at higher compression rates than traditional compression techniques do [15]. This approach has been adopted for satellite imagery, as well. Kong et al. [23] have proposed a spectral-spatial feature-partitioned extraction to process the spectral and spatial contents of images in parallel. Alves de Oliveira et al. [24] have introduced a lightweight variational auto-encoder suitable for on board satellite compression. The authors have then combined onboard compression of satellite images with de-noising [25], which otherwise would be performed at the ground stations. Kong et al. [26] have described a multi-spectral image compression framework based on residual networks to deal with spectral and spatial redundancy. In contrast to our work, these approaches focus only on source compression and do not take into account communication in form of channel coding and modulation.

## III. SYSTEM MODEL

In this paper, we assume a single LEO satellite that is used for Earth observation purposes and transmits acquired image data to a single ground station. We further assume that the available communication channel is bandwidth constrained to an extent that requires data compression in order for transmissions to keep up with the amount of generated sensor data.

In the following, we will give a brief introduction to Sentinel-2, a well known Earth observation mission that we take as basis for our evaluation, and we give an overview of satellite hardware and its suitability to deploy neural networks. Finally, we introduce the channel model we employ for the design of our transmission scheme.

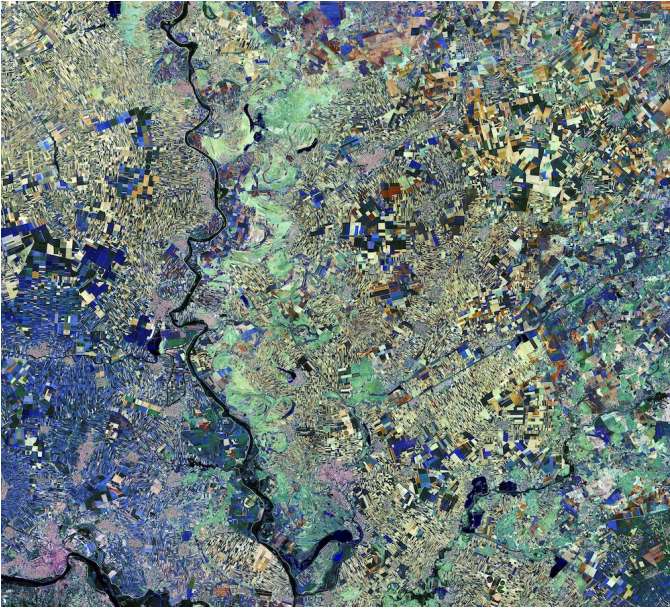


Fig. 1. An example image from the Sentinel-2 mission showing the region of Vojvodina, Serbia (Credit: processed by ESA, CC BY-SA 3.0 IGO).

### A. Earth observation using small satellites

Due to their small size and relative cost efficiency, small satellites are increasingly used for earth observation tasks. Common use cases include agricultural monitoring, emergencies management, land cover classification, and water quality estimates. For training our neural network approach and for our evaluation, we use Earth observation data acquired from the European space agency’s Sentinel-2 mission [27]. Sentinel-2 is an Earth observation mission from the Copernicus program. Its satellites capture optical data with a relatively high resolution of 10 m to 60 m, and they operate in low Earth orbit (LEO). Each satellite uses a multi-spectral instrument to capture not only visible light but also near infrared and short wave infrared spectra. Table I gives an overview of the 13 captured bands, with wavelengths ranging from approximately 430 nm to 2290 nm. The radiometric brightness ranges up to 4096 with a resolution of 12 bit. Figure 1 shows an example image from the Sentinel-2 mission taken in 2016 [28], which has been recolored by analyzing the multi-spectral bands to indicate varying vegetative states, such as freshly ploughed land or different stages of crop growth or chlorophyll and water contents.

### B. Deploying neural networks onboard small satellites

Since the small size of satellites limits their energy budget, it is necessary to consider energy constraints when deploying neural networks onboard of satellites. In addressing the system’s deployability and energy consumption, we turn to several key studies and missions.

The detection of cargo ships on the ocean from satellite imagery has been tested using an Nvidia TX2 SoC, which not only fits within CubeSat limitations but also sustains a

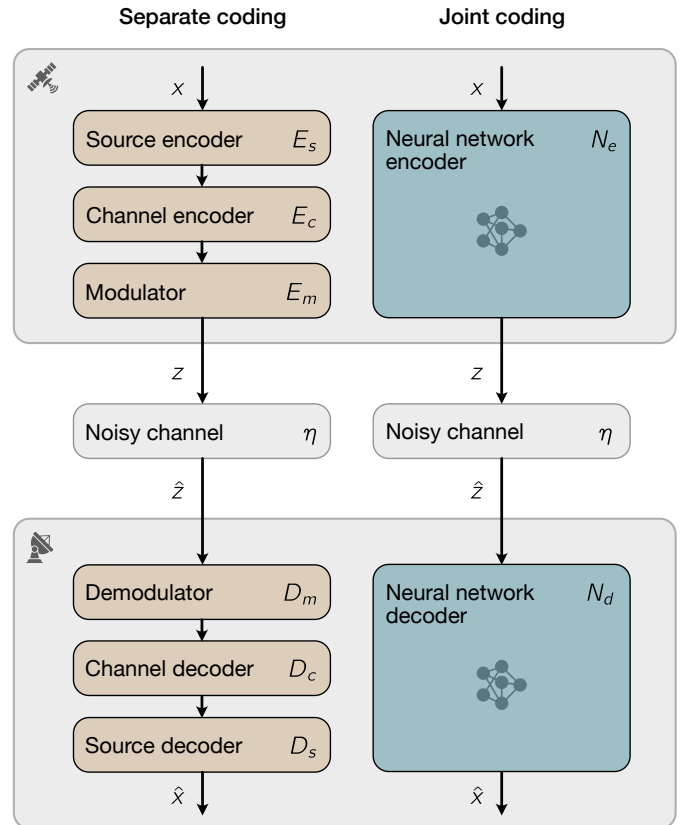


Fig. 2. Comparison between the traditional communication model using separate coding and our joint coding approach.

total power envelope of 7.5 W, making it compatible with small satellite missions [29]. The Intel Movidius Myriad 2 and STM32 Microcontroller, both low-power processors, have successfully executed star identification tasks using neural networks with a power usage of 0.89–1.08 W for Myriad and 1.15–1.2 W for STM32 [30]. On the International Space Station (ISS), deep learning models were evaluated on the Qualcomm Snapdragon 855 and Intel Movidius Myriad X processors, further underlining the feasibility of running a neural network onboard of satellites [31]. A variety of models were tested that were trained on images from Earth and Mars. In particular, rather large standard ML models, such as VGG19 [32] and ResNet50 [33], were used. Moreover, the practical deployment of ML models onboard small satellites was tested in the  $\Phi$ -Sat mission via the use of Intel Movidius Myriad 2 for onboard cloud detection [34].

### C. Communication model

We assume a communication model where the goal is to transmit the multi-spectral images acquired by the satellite to the ground station via a bandwidth-constraint channel. In a traditional transmission scheme, three components are considered separately, as shown in Figure 2 on the left side. We represent the input image  $x \in \mathbb{R}^n$  as an  $n$ -dimensional vector. The image  $x$  is first compressed with a source encoder

$E_s$ , which removes the redundancies present in the input data and potentially introduces a lossy compression. For instance, the lossy image compression mechanism JPEG 2000 is often used in existing satellite communication protocols [7]. Then, to ensure a reliable transmission over a noisy channel, a channel encoder  $E_c$  is applied. The channel coder adds redundancy to protect the transmission against corruption, for instance, using LDPC codes. Finally, during the modulation step, the output of the channel encoder is mapped to complex-valued samples  $z \in \mathbb{C}^k$  using the modulation scheme  $E_m$ . The resulting channel symbols are transmitted to the ground station via a noisy channel  $\eta$ . Due to packet loss, the ground station receives a potentially corrupted vector of signals  $\hat{z}$ . Once received, the signal is first demodulated and mapped to bits using the demodulation scheme  $D_m$ . Then possibly corrupted data is restored with the help of a channel decoder  $D_c$ . Finally, the data is decompressed with a source decoder  $D_s$  to obtain a representation  $\hat{x}$  that approximates the original image data.

For our joint coding approach (see right part of Figure 2), we replace the individual encoding and decoding steps with an encoder  $N_e$  and a joint decoder  $N_d$ , which jointly optimize source (de)coding, channel (de)coding, and (de)modulation, as we will explain in the following section.

#### IV. JOINT SOURCE AND CHANNEL CODING FOR SMALL SATELLITE APPLICATIONS

In order to use a neural network for joint encoding, we need to define a network architecture, which directly maps the input image  $x$  to its channel representation  $z$ . Our main goal is to find an encoder-decoder architecture that adapts well to a range of different channel conditions, as often observed in satellite communications. In contrast to this joint approach, separate source and channel codes are usually chosen based on specific assumptions about the channel quality. Therefore, their performance can degrade quickly when channel conditions differ from those expected. Channel conditions in satellite communications, in particular, can vary quickly due to satellite movement, changing weather conditions, and wireless interference at the ground stations. This is especially true for high-frequency communication, which is required to achieve the high data rates necessary to transmit multi-spectral images. A similar problem occurs when the channel conditions are better than expected. In this case, a system using separate encoders cannot improve its performance and the quality of the received data remains the same [14].

To design the joint system, we use an encoder-decoder neural network architecture. Essentially, the encoder part of the network translates input image data directly to its channel representation, and the decoder translates the channel representation back to the reconstructed image data. We train the model using multi-spectral images from the Sentinel-2 dataset to optimize its performance for satellite applications and use the reconstructed image's quality as reward metric during the training. Once the training is completed, we can use the encoder part of the trained network on the satellite and the decoder part on the ground station to obtain the joint

encoder and decoder, respectively. To parametrize the network, we calculate SNR values based on suitable assumptions about the link budget for a satellite-to-ground-station link.

Next, we explain the network architecture and how we calculate suitable SNR values based on the link budget in detail.

##### A. Neural network architecture

Our neural network architecture is based on the deep joint source and channel coding (DJSCC) approach [14], which we adapt for the satellite communication setting. Namely, we design a suitable neural network architecture for encoding and decoding of multi-spectral satellite images.

The system consists of a neural network serving as encoder, which combines source coding, channel coding, and modulation. That is, the input image  $x \in \mathbb{R}^n$  is mapped directly to channel input symbols  $z \in \mathbb{C}^k$ . The ratio  $k/n$  ( $k < n$ ) determines the compression ratio of the model. The second neural network, the decoder, receives as input the transmitted and possibly corrupted vector  $\hat{z} \in \mathbb{C}^k$  and restores the image  $\hat{x} \in \mathbb{R}^n$ .

The proposed architecture is presented in Figures 3 and 4. We combine a number of layers to form both the encoder network  $N_e$  and the decoder network  $N_d$ . The network architecture is based on ResNet [35], which is commonly used for image classification. We adapt the network to output channel-coded symbols by replacing ResNet's dense layers, which normally perform the image classification, with a suitable layer structure for the joint encoding. Similarly, a reversed network architecture is used for decoding. During training, both the encoder and decoder part are trained jointly, and a non-trainable layer in between is used to model the communication channel. During operation, the encoder and decoder parts are used separately on the satellite and ground station, respectively. In the following, we explain the encoder and decoder network architectures in more detail.

The encoder consists of four residual blocks with 256 filters and a kernel size of  $3 \times 3$ . The last layer is a convolutional layer consisting of  $c$  filters, where  $c$  is determined by the compression ratio  $k/n$ . We use a parameterized rectified linear unit (PReLU) as activation function, which generalizes the traditional ReLU by introducing a learnable parameter, which improves predictions. The output of the encoder is combined into a vector  $\tilde{z}$  of  $k$  complex-valued numbers representing the channel symbols. Then the vector is normalized as follows to ensure that the average transmit power constraint  $P$  is satisfied:

$$z = \sqrt{kP} \frac{\tilde{z}}{\sqrt{\tilde{z}^* \tilde{z}}}, \quad (1)$$

where  $\tilde{z}^*$  denotes the conjugate transpose of  $\tilde{z}$ . The average transmit power constraint  $P$  can be intuitively understood as the maximum power that can be transmitted over the channel on average, varying depending on the channel conditions, such as distance, interference, and noise.

The next layer is a non-trainable channel layer that introduces noise to  $z$  for a given SNR in order to obtain the

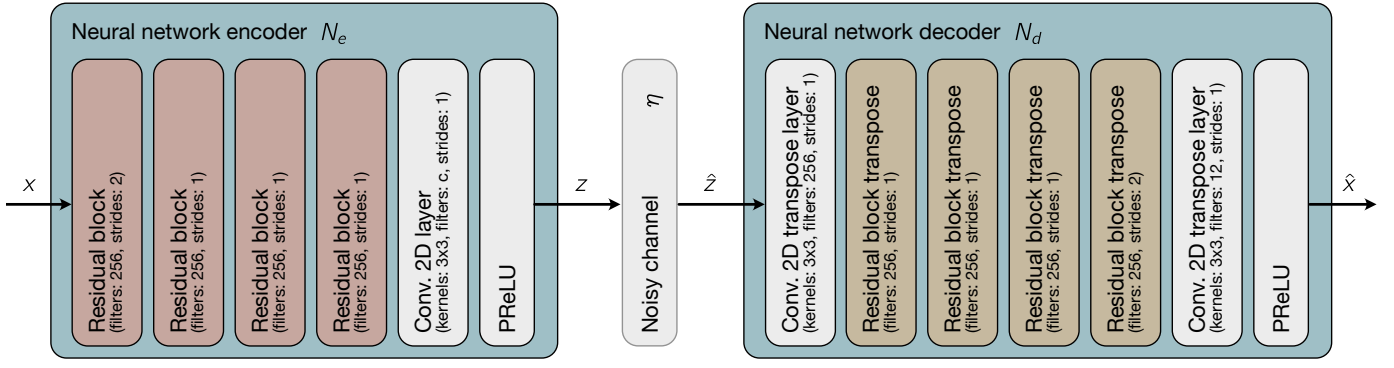


Fig. 3. Encoder-decoder neural network architecture overview.

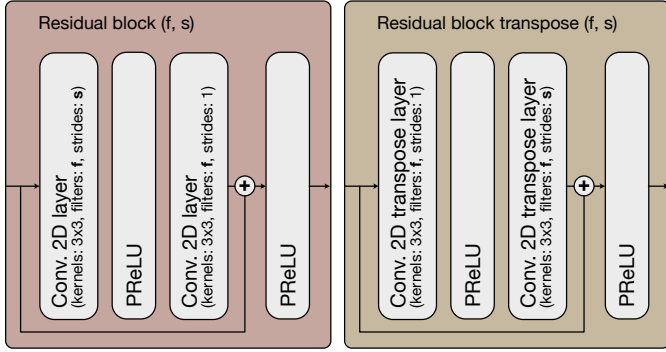


Fig. 4. Residual block architectures used in the encoder and decoder parts of the neural network architecture.

noisy signal  $\hat{z}$ . To explain the concept, we use an additive white Gaussian noise (AWGN) channel and describe how it is modelled as a layer in our encoder-decoder architecture; we will explain how to obtain the required SNR values in Section IV-B. First, we compute the signal power based on the normalized channel symbols  $z$ :

$$P_{\text{sig}} = \frac{1}{k} \sum_{i=0}^{k-1} |z_i|^2 \quad (2)$$

Then, we determine the required noise power spectral density:

$$N_0 = \frac{P_{\text{sig}}}{10^{\frac{\text{SNR}}{10}}} \quad (3)$$

$N_0$  is used to compute the noise power:

$$\sigma^2 = \frac{N_0}{2} \quad (4)$$

Finally, we generate a complex-valued noise vector  $n$  using the normal distribution and compute the resulting noisy output:

$$n = \sigma \times [\mathcal{N}(0, 1) + j * \mathcal{N}(0, 1)] \quad (5)$$

$$\hat{z} = z + n \quad (6)$$

Similar to encoder, the decoder consists of a convolutional transpose layer, four residual transpose blocks, another convolutional transpose layer, and a PReLU activation function. The decoder takes  $\hat{z}$  as input and restores an approximation of the

image  $\hat{x}$ . During training, we use the average mean squared error (MSE) as loss function, which is defined as:

$$\mathcal{L} = \text{MSE} = \frac{1}{N} \sum_{i=1}^N d(x_i, \hat{x}_i), \quad (7)$$

where  $N$  is the number of samples and  $d(x, \hat{x}) = \|x - \hat{x}\|^2$  denotes the MSE distortion.

During evaluation, use the peak signal-to-noise ratio (PSNR) as a metric to determine the quality of the reconstructed image as follows:

$$\text{PSNR} = 10 \log_{10} \frac{\text{MAX}^2}{\text{MSE}}, \quad (8)$$

where MAX is the maximum possible pixel value.

Intuitively, PSNR expresses the ratio between the maximum possible signal value and the distorting noise that reduces its quality. The metric is often used to measure the reconstruction quality of lossy compression codecs, as it approximates human perception of the reconstruction quality.

### B. Link budget analysis

In order to model the transmission channel between the satellite and ground station, we need to determine the SNR values that can be assumed. Therefore, we perform a link budget analysis in order to evaluate the communication link quality of LEO satellites with their ground stations. In the following, we summarize the basic calculations required to compute SNRs.

The expected SNR can be computed with the help of the following formula:

$$\text{SNR} = P_t + G_t + G_r - L - N, \quad (9)$$

where  $P_t$  is the transmitted power,  $G_t$  and  $G_r$  are the transmitter and the receiver antenna gains, respectively,  $L$  is the path loss, and  $N$  is the thermal noise. All quantities are calculated in decibel. The  $P_t$ ,  $G_t$  and  $G_r$  are input parameters depending on the particular equipment in use.

Finally,  $L$  and  $N$  need to be estimated based on the assumed environment.  $L$  can be determined from the Friis transmission formula as follows:

$$L = \frac{1}{G_t G_r} \left( \frac{4\pi d f}{c} \right)^2, \quad (10)$$

where  $d$  is the slant range, that is, the distance between the satellite and the ground station,  $f$  is the carrier frequency, and  $c = 299792458$  m/s is the speed of light.

To compute the slant range  $d$ , two parameters are necessary: the orbit height  $h$  and the elevation angle  $\epsilon_0$ . The latter describes how high the position of the satellite is above the horizon. Assuming the satellite flying in an overhead trajectory, the slant range can then be computed using the following formula [36]:

$$d = R_E \left( \sqrt{\left( \frac{h + R_E}{R_E} \right)^2 - \cos^2 \epsilon_0} - \sin \epsilon_0 \right), \quad (11)$$

where  $R_E = 6378$  km is the radius of Earth. The elevation angle  $\epsilon_0$  and hence the slant range  $d$  are changing over time due to the high relative movement speed of the satellite. For our evaluation, we therefore consider a number of different elevation angles, for which we calculate SNR values and train corresponding encoder and decoder networks. In practice, these networks can be switched based on tracking of the satellite, or they can be merged into a combined encoder and decoder network for multiple angles [37].

Finally, the thermal noise  $N$  can be computed as

$$N = k \cdot T \cdot B, \quad (12)$$

where  $k = 1.380649 \cdot 10^{-23}$  is Boltzmann's constant,  $T$  is the noise temperature, and  $B$  is the bandwidth.  $T$  can be estimated as

$$T = T_a + T_e, \quad (13)$$

where  $T_a$  is the antenna temperature, which is difficult to estimate, since it depends on weather conditions and noise level around the ground station. We assume  $T_a = 290$  K as a suitable approximation.  $T_e$  is the receiver noise temperature, that is, the noise caused by the electronics of the receiver.  $T_e$  can be estimated as

$$T_e = T_0 (F_{\text{sys}} - 1), \quad (14)$$

where  $T_0 = 290$  K is the reference temperature, and  $F_{\text{sys}}$  is the receiver's noise figure.

By using these formulae, we can approximate suitable SNR values that we plug into the encoder-decoder network's channel layer during trainings to obtain the best possible PSNR values for the given channel conditions.

## V. EVALUATION

In this section, we evaluate the JSCC-SAT approach by comparing it to JPEG 2000, which is commonly used for compression of satellite images [7]. We use the BigEarth dataset [38], [39], which is a collection of 590,326 multi-spectral images acquired by Sentinel-2, as explained in Section III-A. More specifically, we use a subset of all images contained in the dataset, which cover the area of Serbia in the summer months. We remove cloudy images from the dataset with the help of a script provided by the BigEarthNet authors,

TABLE II  
CHANNEL PARAMETERS

Parameter	Value
Orbit height	150 km
Carrier frequency	2150 MHz
Transmitted power	1 W
Satellite antenna gain	6 dBi
Ground station antenna gain	35 dBi
Receive channel bandwidth	750 kHz
Noise figure	2 dB

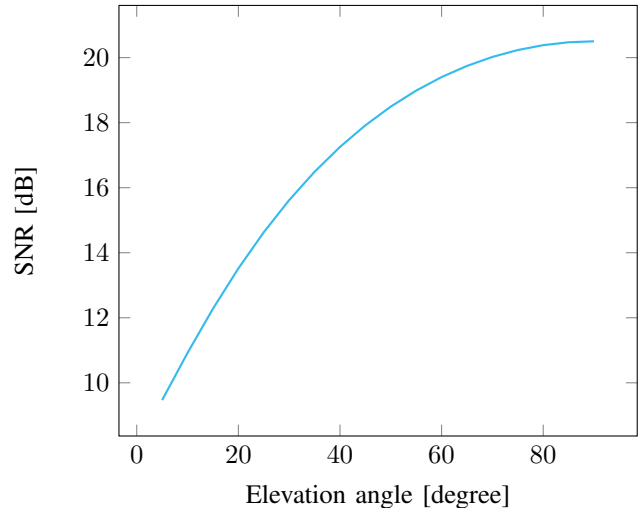


Fig. 5. SNR values for different elevation angles.

following common evaluation practices. In total, 14,439 multi-spectral images remain in the filtered dataset. Each multi-spectral image is represented by 12 individual files, where each file encodes one of the bands using the lossless tag image file format (TIFF) format. The dataset was then further divided into training, validation, and test sets. Since the individual bands in the dataset have different resolutions (see Table I), we used cubic interpolation to resize all image files to the same size. The dataset contains 12 bands. Sentinel-2's band 10 contains information about clouds is not included in the dataset, since it is not useful for training. Finally, the pixel values were normalized so that they are between 0 and 1.

To apply JSCC-SAT, we implement the neural network architecture described in Section IV using Keras<sup>1</sup> and TensorFlow.<sup>2</sup> The batch size was set to 32, and the learning rate was set to  $10^{-3}$  and adjusted to  $10^{-4}$  after 500 epochs. We used Adam as optimizer, which is a form of stochastic gradient descent. A separate neural network was trained till convergence for each SNR value.

We further computed the SNR values using the formulas described in Section IV-B and the parameters from Table II. As main varying factor, we consider the satellites elevation angle relative to the ground station to cover a wide range of

<sup>1</sup>Website: <https://keras.io/>

<sup>2</sup>Website: <https://www.tensorflow.org/>

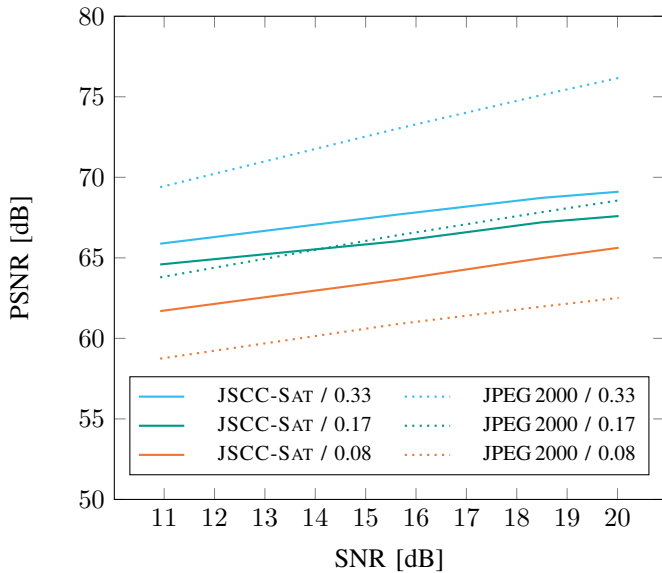


Fig. 6. JSCC-SAT vs. JPEG 2000 under optimal conditions for  $k/n = \{0.08, 0.17, 0.33\}$ .

possible transmission environments. Figure 5 shows the SNRs depending on the elevation angle. A separate neural network is trained for each SNR value.

We consider two simulation scenarios:

- 1) We compare JSCC-SAT against JPEG 2000 with maximum rate for source compression, that is, assuming guaranteed reliable transmission according to Shannon's separation theorem, to obtain an upper bound for the performance of JPEG 2000.
- 2) We compare JSCC-SAT against JPEG 2000 with additional channel coding using LDPC for a more realistic upper bound.

For both scenarios, we compare the achieved image quality measured using PSNR values for various realistic SNR values. The higher the PSNR values of the reconstructed images, the better the image quality.

First, we compare JSCC-SAT with JPEG 2000 for different compression ratios  $k/n = \{0.33, 0.17, 0.08\}$ . We compute an upper bound for the maximum data rate at which the data can be compressed and transmitted using Shannon's separation theorem [8]:

$$R_{\max} = \frac{k}{n}C, \quad (15)$$

where  $C$  denotes the channel capacity, which can be computed for an AWGN channel with the help of the following formula:

$$C = \log_2(1 + \text{SNR}). \quad (16)$$

Based on this calculation, we can obtain PSNR values for JPEG 2000 assuming that no packet loss occurs, therefore constituting an upper bound.

The results are presented in Figure 6. The  $x$ -axis shows different SNR values, and the  $y$ -axis shows resulting PSNR

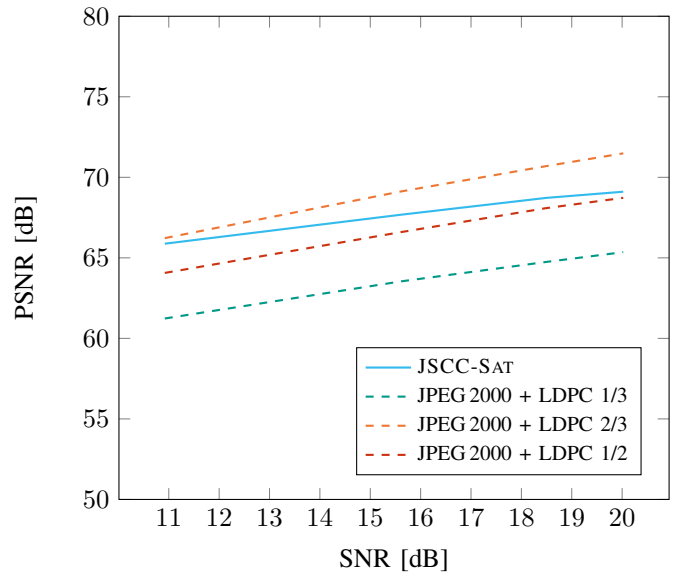


Fig. 7. JSCC-SAT vs. JPEG 2000 + LDPC for  $k/n = 0.33$ .

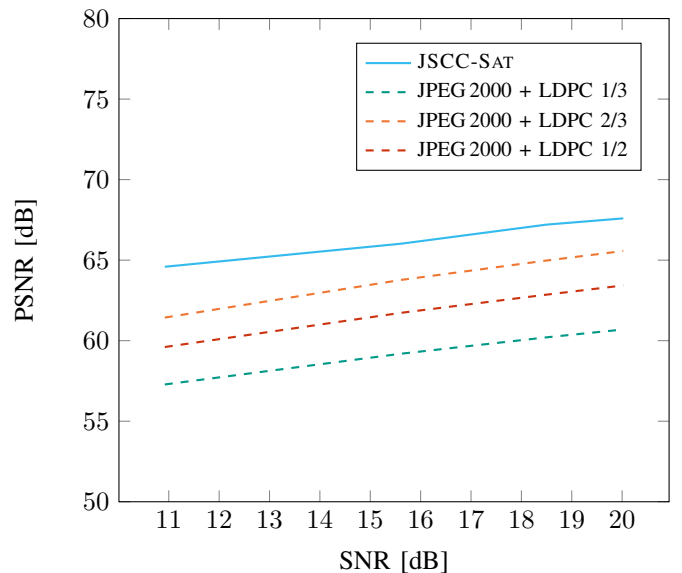


Fig. 8. JSCC-SAT vs. JPEG 2000 + LDPC for  $k/n = 0.17$ .

values after the image data has been transmitted and reconstructed at the receiver. It becomes clear that JSCC-SAT considerably outperforms JPEG 2000 for  $k/n = 0.08$ . In case of  $k/n = 0.17$ , JSCC-SAT performs better for low SNR values. JPEG 2000, however, performs slightly better for higher SNR values with this compression ratio. Finally, JPEG 2000 performs better across all SNR values when  $k/n = 0.33$ . Note again that the results for JPEG 2000 describe a theoretic upper bound that is not achievable in practice.

To provide a more realistic upper bound, we apply channel coding after compressing the data with JPEG 2000. To imple-

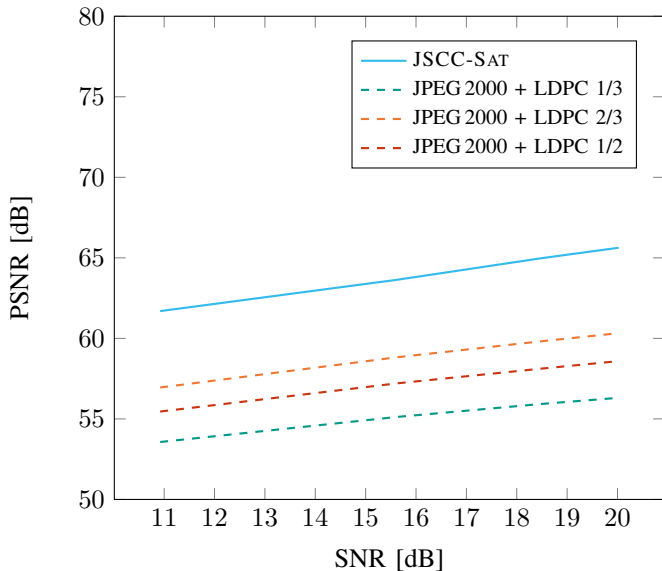


Fig. 9. JSCC-SAT vs. JPEG 2000 + LDPC for  $k/n = 0.08$ .

ment channel coding, we use the LDPC codec with code rates 1/3, 1/2, and 2/3 in our evaluation. The results are shown in Figures 7 to 9. Each figure shows a single compression ratio  $k/n$ , for which we compare JSCC-SAT against JPEG 2000 + LDPC with the three different code rates applied. Like in Figure 6, the  $x$ -axis shows the SNR values and the  $y$ -axis the resulting reconstructed image quality measured in PSNR.

In this more realistic scenario, our JSCC approach significantly outperforms JPEG 2000 + LDPC for all code rates for compression ratios  $k/n = 0.08$  and  $k/n = 0.17$ . JSCC-SAT also performs better for code rates 1/3 and 1/2 for  $k/n = 0.33$ . The only parameter combination where JPEG 2000 + LDPC outperforms JSCC-SAT is with code rate 2/3 and compression ratio  $k/n = 0.33$ . This parameter combination represents the lowest compression (i.e., highest resulting transmission file size) combined with the highest channel code rate. This combination provides the lowest data rate and thus may incur prohibitive overhead given the short visibility periods between satellites and ground stations.

Summarizing, we have shown that JSCC-SAT outperforms JPEG 2000 even under ideal conditions for some compression ratios, and it outperforms JPEG 2000 with added LDPC for all but the most unfavorable data rates.

## VI. CONCLUSION

Small satellites have recently become more and more popular due to their efficiency and support for a wide range of Earth observation applications. In contrast to larger, more costly satellites, LEO satellites pose a number of additional communication challenges.

In particular, efficient source and channel coding schemes are required in order to cope with the large amount of generated image data that needs to be transmitted over a channel with small capacity. While Shannon's theory states

that separate mechanisms can be combined to achieve optimal results, these theoretical bounds cannot be achieved in practice.

We have considered a joint source-and-channel coding approach based on neural networks that combines source coding, channel coding, and modulation for satellite applications. Our evaluation results show that JSCC-SAT is able to outperform transmission using JPEG 2000 and LDPC for a number of realistic compression ratios covering a range of expectable SNRs. Thereby we have shown the potential to apply neural networks when designing transmission mechanisms for satellite applications to achieve more robust and flexible communication protocols.

In future work, we aim to extend our mechanism to more complex multi-satellite scenarios, where neural networks could be used to jointly optimize communication across these satellites, and we plan to investigate how to combine the trained neural networks into a single network covering a range of SNRs. Moreover, we currently focus on CNN models, which cover a wide range of common satellite applications based on vision tasks. As an extension of our work, we see the potential to adapt our mechanism to other neural network model types that support non-vision tasks.

## REFERENCES

- [1] *CubeSat design specification*, The CubeSat Program, Cal Poly SLO, 2022, rev. 14. [Online]. Available: <https://www.cubesat.org/cubesatinfo>
- [2] J. Wang, D. Li, W. Cao, X. Lou, A. Shi, and H. Zhang, "Remote sensing analysis of erosion in Arctic coastal areas of Alaska and eastern Siberia," *Remote Sensing*, vol. 14, no. 3, 2022.
- [3] "Radix," accessed: 2023-04-28. [Online]. Available: [https://space.skyrocket.de/doc\\_sdat/radix.htm](https://space.skyrocket.de/doc_sdat/radix.htm)
- [4] P. Barmpoutis, P. Papaioannou, K. Dimitropoulos, and N. Grammalidis, "A review on early forest fire detection systems using optical remote sensing," *Sensors*, vol. 20, no. 22, 2020.
- [5] "Marco," accessed: 2023-04-28. [Online]. Available: <https://www.jpl.nasa.gov/missions/mars-cube-one-marco>
- [6] C. Nogales, B. Grim, M. Kamstra, B. Campbell, A. Ewing, R. Hance, J. Griffin, and S. Parke, "MakerSat-0: 3D-printed polymer degradation first data from orbit," 08 2018.
- [7] European Space Agency, "Sentinel-2 user handbook," 2015. [Online]. Available: [https://sentinel.esa.int/documents/247904/685211/sentinel-2\\_user\\_handbook](https://sentinel.esa.int/documents/247904/685211/sentinel-2_user_handbook)
- [8] T. M. Cover and J. A. Thomas, *Elements of Information Theory*. Wiley-Interscience, 1991.
- [9] V. Kostina and S. Verdú, "Lossy joint source-channel coding in the finite blocklength regime," *IEEE Transactions on Information Theory*, vol. 59, no. 5, pp. 2545–2575, 2013.
- [10] W. Yu, Z. Sahinoglu, and A. Vetro, "Energy efficient jpeg 2000 image transmission over wireless sensor networks," in *IEEE Global Telecommunications Conference, 2004. GLOBECOM '04.*, vol. 5, 2004, pp. 2738–2743 Vol.5.
- [11] S. Appadwedula, D. Jones, K. Ramchandran, and L. Qian, "Joint source channel matching for a wireless image transmission," in *Proceedings 1998 International Conference on Image Processing. ICIP98 (Cat. No.98CB36269)*, vol. 2, 1998, pp. 137–141 vol.2.
- [12] J. Cai and C. W. Chen, "Robust joint source-channel coding for image transmission over wireless channels," *IEEE Transactions on Circuits and Systems for Video Technology*, vol. 10, no. 6, pp. 962–966, 2000.
- [13] T.-Y. Tung, D. B. Kurka, M. Jankowski, and D. Gündüz, "Deepjpsc-q: Channel input constrained deep joint source-channel coding," in *ICC 2022 - IEEE International Conference on Communications, 2022*, pp. 3880–3885.
- [14] E. Boursoulatzé, D. B. Kurka, and D. Gunduz, "Deep joint source-channel coding for wireless image transmission," *IEEE Transactions on Cognitive Communications and Networking*, vol. 5, no. 3, pp. 567–579, sep 2019.



- [15] Y. Hu, W. Yang, Z. Ma, and J. Liu, "Learning end-to-end lossy image compression: A benchmark," *IEEE Transactions on Pattern Analysis and Machine Intelligence*, vol. 44, no. 8, pp. 4194–4211, 2022.
- [16] M. Yang and H.-S. Kim, "Deep joint source-channel coding for wireless image transmission with adaptive rate control," 2021.
- [17] D. B. Kurka and D. Gündüz, "Bandwidth-agile image transmission with deep joint source-channel coding," *IEEE Transactions on Wireless Communications*, vol. 20, no. 12, pp. 8081–8095, 2021.
- [18] O. Y. Bursalioglu, G. Caire, and D. Divsalar, "Joint source-channel coding for deep space image transmission using rateless codes," in *2011 Information Theory and Applications Workshop*, 2011, pp. 1–10.
- [19] F. A. Aoudia and J. Hoydis, "Model-free training of end-to-end communication systems," *IEEE Journal on Selected Areas in Communications*, vol. 37, no. 11, pp. 2503–2516, 2019.
- [20] T.-Y. Tung, D. B. Kurka, M. Jankowski, and D. Gündüz, "Deepjsec-q: Channel input constrained deep joint source-channel coding," in *JCC 2022 - IEEE International Conference on Communications*, 2022, pp. 3880–3885.
- [21] M. Yang, C. Bian, and H.-S. Kim, "Deep joint source channel coding for wireless image transmission with ofdm," 2021.
- [22] Z. Xuan and K. Narayanan, "Deep joint source-channel coding for transmission of correlated sources over awgn channels," in *ICC 2021 - IEEE International Conference on Communications*, 2021, pp. 1–6.
- [23] F. Kong, K. Hu, Y. Li, D. Li, and S. Zhao, "Spectral-spatial feature partitioned extraction based on CNN for multispectral image compression," *Remote Sensing*, vol. 13, no. 1, p. 9, Dec. 2020.
- [24] V. A. de Oliveira, M. Chabert, T. Oberlin, C. Poulliat, M. Bruno, C. Latry, M. Carlavan, S. Henrot, F. Falzon, and R. Camarero, "Reduced-complexity end-to-end variational autoencoder for on board satellite image compression," *Remote Sensing*, vol. 13, no. 3, p. 447, Jan. 2021.
- [25] V. Alves de Oliveira, M. Chabert, T. Oberlin, C. Poulliat, M. Bruno, C. Latry, M. Carlavan, S. Henrot, F. Falzon, and R. Camarero, "Satellite image compression and denoising with neural networks," *IEEE Geoscience and Remote Sensing Letters*, vol. 19, pp. 1–5, 2022.
- [26] F. Kong, S. Zhao, Y. Li, D. Li, and Y. Zhou, "A residual network framework based on weighted feature channels for multispectral image compression," *Ad Hoc Networks*, vol. 107, p. 102272, Oct. 2020.
- [27] "sentinel2," accessed: 2023-04-28. [Online]. Available: <https://sentinel.esa.int/web/sentinel/missions/sentinel-2>
- [28] ESA, "Vojvodina, Serbia," 2016. [Online]. Available: [https://www.esa.int/ESA\\_Multimedia/Images/2017/04/Vojvodina\\_Serbia](https://www.esa.int/ESA_Multimedia/Images/2017/04/Vojvodina_Serbia)
- [29] A. P. Arechiga, A. J. Michaels, and J. T. Black, "Onboard image processing for small satellites," in *NAECON 2018 - IEEE National Aerospace and Electronics Conference*, 2018, pp. 234–240.
- [30] S. Agarwal, E. Hervas-Martin, J. Byrne, A. Dunne, J. Luis Espinosa-Aranda, and D. Rijlaarsdam, "An evaluation of low-cost vision processors for efficient star identification," *Sensors*, vol. 20, no. 21, 2020. [Online]. Available: <https://www.mdpi.com/1424-8220/20/21/6250>
- [31] E. Dunkel, J. Swope, Z. Towfic, S. Chien, D. Russell, J. Sauvageau, D. Sheldon, J. Romero-Cañás, J. L. Espinosa-Aranda, L. Buckley, E. Hervas-Martin, M. Fernandez, and C. Knox, "Benchmarking deep learning inference of remote sensing imagery on the qualcomm snapdragon and intel movidius myriad x processors onboard the international space station," in *IGARSS 2022 - 2022 IEEE International Geoscience and Remote Sensing Symposium*, 2022, pp. 5301–5304.
- [32] K. Simonyan and A. Zisserman, "Very deep convolutional networks for large-scale image recognition," in *3rd International Conference on Learning Representations, ICLR 2015, San Diego, CA, USA, May 7-9, 2015, Conference Track Proceedings*, Y. Bengio and Y. LeCun, Eds., 2015. [Online]. Available: <http://arxiv.org/abs/1409.1556>
- [33] K. He, X. Zhang, S. Ren, and J. Sun, "Deep residual learning for image recognition," in *2016 IEEE Conference on Computer Vision and Pattern Recognition (CVPR)*, 2016, pp. 770–778.
- [34] G. Giuffrida, L. Fanucci, G. Meoni, M. Batič, L. Buckley, A. Dunne, C. van Dijk, M. Esposito, J. Hefele, N. Verduyssen, G. Furano, M. Pastena, and J. Aschbacher, "The  $\phi$ -sat-1 mission: The first on-board deep neural network demonstrator for satellite earth observation," *IEEE Transactions on Geoscience and Remote Sensing*, vol. 60, pp. 1–14, 2022.
- [35] K. He, X. Zhang, S. Ren, and J. Sun, "Deep residual learning for image recognition," *arXiv preprint 1512.03385*, 2015.
- [36] O. Popescu, J. S. Harris, and D. C. Popescu, "Designing the communication sub-system for nanosatellite cubesat missions: Operational and implementation perspectives," in *SoutheastCon 2016*, 2016, pp. 1–5.
- [37] M. Yang and H.-S. Kim, "Deep joint source-channel coding for wireless image transmission with adaptive rate control," 2021.
- [38] G. Sumbul, M. Charfuelan, B. Demir, and V. Markl, "BigEarthNet: A large-scale benchmark archive for remote sensing image understanding," in *IEEE International Geoscience and Remote Sensing Symposium*, Yokohama, Japan, 2019, pp. 5901–5904.
- [39] G. Sumbul, A. de Wall, T. Kreuziger, F. Marcelino, H. Costa, P. Benevides, M. Caetano, B. Demir, and V. Markl, "BigEarthNet-MM: A large-scale, multimodal, multilabel benchmark archive for remote sensing image classification and retrieval [software and data sets]," *IEEE Geoscience and Remote Sensing Magazine*, vol. 9, no. 3, pp. 174–180, Sep. 2021.